Multi-Class Classification of Upper Limb Movements With Filter Bank Task-Related Component Analysis

Hao Jia, Fan Feng, Cesar F. Caiafa, Feng Duan, *Member, IEEE*, Yu Zhang, Zhe Sun, and Jordi Solé-Casals

***Abstract*—The classification of limb movements can provide with control commands in non-invasive brain-computer interface. Previous studies on the classification of limb movements have focused on the classification of left/right limbs; however, the classification of different types of upper limb movements has often been ignored despite that it provides more active-evoked control commands in the brain-computer interface. Nevertheless, few machine learning method can be used as the state-of-the-art method in the multi-class classification of limb movements. This work focuses on the multi-class classification of upper limb movements and proposes the multi-class filter bank task-related component analysis (mFBTRCA) method, which consists of three steps: spatial filtering, similarity measuring and filter bank selection. The spatial filter, namely the task-related component analysis, is first used to remove noise from EEG signals. The canonical correlation measures the similarity of the spatial-filtered signals and is used for feature extraction. The correlation features are extracted from multiple low-frequency filter banks. The minimum-redundancy maximum-relevance selects the essential features from all the correlation features, and finally, the support vector machine is used to classify the selected features. The proposed method compared against previously used models is evaluated using two datasets. mFBTRCA achieved a classification accuracy of 0.4193 $\pm$ 0.0780 (7 classes) and 0.4032 $\pm$ 0.0714 (5 classes), respectively, which improves on the best accuracies achieved using the compared methods (0.3590 $\pm$ 0.0645 and 0.3159 $\pm$ 0.0736, respectively). The proposed method is expected to provide more control commands in the applications of non-invasive brain-computer interfaces.**

***Index Terms*—Brain-computer interface, electroencephalogram, movement-related cortical potential, upper limb movement, pattern recognition.**

Manuscript received 13 October 2022; revised 8 February 2023 and 21 April 2023; accepted 11 May 2023. Date of publication 25 May 2023; date of current version 7 August 2023. This work was carried out as part of the doctoral program in Experimental Science and Technology at the University of Vic - Central University of Catalonia. The work of Jordi Solé-Casals was partially supported by the European Cooperation in Science and Technology (COST) through COST Action under Grant CA18106. The work of Cesar F. Caiafa work was supported by under Grants PICT 2020-SERIEA-00457 and PIP 112202101 00284CO (Argentina). This work was supported in part by the National Natural Science Foundation of China (Key Program) under Grant 11932013, and in part by the Tianjin Science and Technology Plan Project under Grant 22PTZWHZ00040. *(Corresponding authors: Feng Duan; Zhe Sun; Jordi Solé-Casals.)*

Hao Jia is with the Data and Signal Processing Research Group, University of Vic-Central University of Catalonia, 08500 Vic, Spain (e-mail: jia.hao@uvic.cat).

Fan Feng is with the College of Artificial Intelligence, Nankai University, Tianjin 300350, China (e-mail: 0bearsuny0@gmail.com).

Cesar F. Caiafa is with the Instituto Argentino de Radioastronomía, CONICET CCT La Plata/CIC-PBA/UNLP, Villa Elisa 1894, Argentina (e-mail: ccaiafa@fi.uba.ar).

Feng Duan is with the Key Laboratory of Brain Science and Intelligent Rehabilitation, College of Artificial Intelligence, Nankai University, Tianjin 300350, China (e-mail: duanf@nankai.edu.cn).

Yu Zhang is with the Department of Bioengineering and the Department of Electrical and Computer Engineering, Lehigh University, Bethlehem, PA 18015 USA (e-mail: yuzhang@lehigh.edu).

Zhe Sun is with the Faculty of Health Data Science, Juntendo University, Urayasu 113-8421, Japan (e-mail: z.sun.kc@juntendo.ac.jp).

Jordi Solé-Casals is with the Data and Signal Processing Research Group, University of Vic - Central University of Catalonia, 08500 Vic, Spain, and also with the Department of Psychiatry, University of Cambridge, CB2 0SZ Cambridge, U.K. (e-mail: jordi.sole@uvic.cat).

The link to the code repository is https://github.com/plustar/Movement-Related-Cortical-Potential.

Digital Object Identifier 10.1109/JBHI.2023.3278747

I. Introduction

A NON-INVASIVE brain-computer interface is a framework that bridges the gap between human brains and external computers [1], [2], [3]. In non-invasive brain computer interface, electroencephalogram (EEG) signals can be recorded from the brain scalp with the acquisition devices. The acquired multi-channel signals can be used to analyze the brain activities and classify the states of the brain, such as left and right limb movements or multiple visual stimuli. These states can be converted to control commands, and thus used to control robots or other external devices [4], [5].

In current research on brain-computer interfaces, brain activities such as motor imagery and steady-state visual evoked potentials are frequently used in human-robot interactions [6], [7]. In motor imagery, the commands are generated by classifying movements of the left/right hand, a foot or the tongue [8], [9], [10], [11]. Compared to the imagination of movement, movement execution refers to the actual movement of limbs and can evoke more distinguished activity in brain signals [12]. In the robot controlling with motor imagery, some subjects prefer to executing the movements instead of imagining the movements [13]. The reason is that the movement execution will provide a stronger response in the brain than the movement imagination. In both the imagined movements and the executed

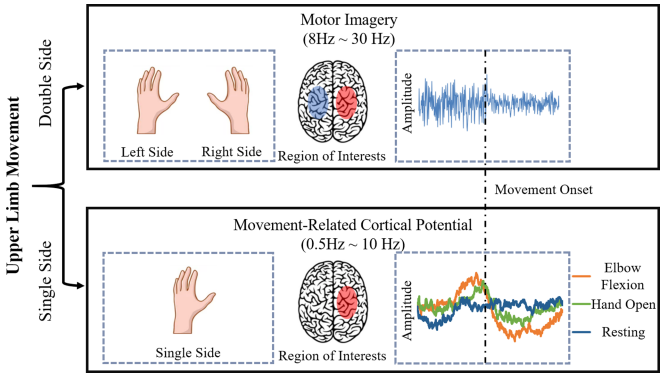

Fig. 1. Differences between double-side and single-side upper limb movement. Motor imagery is used in the classification of double-side movement. In motor imagery, the regions of interest are different between the left side and the right side. The variances of signals change before and after the movement onset. In the single-side classification, the movement-related cortical potential is used. The region of interest is located on a single side of the brain. The amplitude increases and then decreases around the movement onset. The signals' trend also shows differences between motions, such as elbow flexion and hand open. This work focuses on the classification of these single-side motions with movement-related cortical potential.

movement, these active-evoked commands are controlled by human intent. In steady-state visual evoked potentials, the number of commands depends on the number of visual stimuli, and hence there are more control commands [14], [15], [16]. However, the steady-state visual evoked potential is evoked by external visual stimuli. When there are no external visual stimuli, the subjects are unable to generate these control commands intentionally. Thus, the passive-evoked commands limit the application of steady-state visual evoked potentials. Movement-related cortical potential (MRCP) is a brain activity related to limb movement [17]. However, current approaches mainly focused on the binary classification between the limb's resting and movement states or two movement states [18], [19], [20], [21], [22], [23], [24], [25], [26], [27], and very few methods are designed towards multi-class states [12], [28], [29].

Most brain-computer interface studies focus on improving existing classification tasks in motor imagery and steady-state visual evoked potentials [14], [30], [31], [32]. However, research into less exhausting methods for users has been ignored. Limb movements are active-evoked and are controlled by the intent of the subject. The classification of multiple upper limb movements not only is more friendly to users than visual stimuli, but also has more commands if combined with left and right limb classification. However, there are very few methods for the multi-class classification of limb movements such as elbow flexion and pronation of the single-side limb [33], [34], [35], [36].

The classification of limb movements can be divided into two cases, double-side limb movements and single-side limb movements, as shown in Fig. 1. The double-side limb movement is related to the binary left/right limbs in motor imagery. In the multi-class classification, the motions of double-side limb movements are extended to a wide range, including left/right hand movement, left/right foot movement. The single-side limb movement is related to the MRCP signals. The motions include the movement of a single limb, such as elbow flexion, hand close, pronation of the upper limb. The classification of double-side limb movements has obtained many good solutions in the past decades, including the machine-learning methods [37], [38], the deep-learning methods [8], [39], and the source-imaging-based methods [40]. However, the classification of single-side limb movements remains to be developed. Because the data to process in both single-side and double-side movements are the multi-channel EEG signals, the methods in double-side movements can also be used in the single-side movement [25], [36]. However, there are usually performance losses in machine-learning methods and unclear decoding process in deep-learning methods [41]. More related works about the single-side and double-side limb movements are given in the supplementary materials.

In our previous work, we proposed the binary standard task-related component analysis method (bSTRCA) [26]. The bSTRCA follows the processing procedure of spatial filtering and feature extraction. The spatial filter used is the task-related component analysis, and the extracted feature is the canonical correlation coefficient. The bSTRCA method is similar to the matched filter method, as both methods first use spatial filtering to reject the noise in EEG signals and then use a similarity measurement to match the unlabelled EEG signals and the grand average MRCP. However, there are two main differences between the two methods. The first is related to how the spatial filter rejects the noise in the signals. The matched filter method and the bSTRCA method carry out the noise rejection based on the variance and the amplitude of the signals, respectively. MRCP signals are located at the low-frequency band in the frequency domain. In said band, the amplitude of signals mainly reflects the energy change of the signals instead of the variances. The second difference is the role that the similarity measurement plays in the classification. In the matched filter method, the likelihood ratio is the indicator used for classifying the movement and resting states by a threshold criterion. In bSTRCA, correlation coefficients are extracted as features, and a linear discriminant analysis classifier is then used to classify the features. Filter bank selection can further optimize the performance of bSTRCA, and hence the binary filter bank task-related component analysis (bFBTRCA) method was proposed [27]. However, bFBTRCA is not available for multi-class classification because the framework of bSTRCA was initially designed for binary classification.

In this work, we aim to migrate the structure of the bSTRCA method to the multi-class standard task-related component analysis (mSTRCA). Furthermore, we propose the multi-class filter bank task-related component analysis (mFBTRCA) method by incorporating filter bank selection into mSTRCA. The proposed method can be used in the multi-class classification task of single-side limb movements. The proposed method first divides MRCP signals in the low-frequency bands into multiple filter banks. In each filter banks, the multi-channel signals are optimized with the spatial filter. Correlation features are extracted from the optimized features. The correlation features are concatenated and then classified with the support vector machine classifier.

The work firstly explains the decoding of MRCP signals as the rejection of unrelated noises and the measurement of similarity. The mFBTRCA method has a simple structure and shows better performance to other machine-learning and deep-learning methods. This method also extends the use of a TRCA-based method to the context of limb movement.

The structure of this work is as follows. In Section II, the dataset description and details on how the dataset is preprocessed are given. This section also includes a description on the structure of the mFBTRCA method. In Section III, the performance of mFBTRCA is evaluated in the binary classification cases. The proposed method is also compared against other benchmark methods in the multi-class cases. In Section IV, a discussion is given on how the mFBTRCA method uses the information from the MRCP signals, and the bottleneck of mFBTRCA in the multi-class limb movement classifications is also touched upon. Finally, conclusions are given in Section V. A list of acronyms used in this work is included in the supplementary materials to support the reading of the manuscript.

II. Method

A. Dataset Description

Two public EEG datasets (namely datasets I and II) were used to evaluate the performance of the proposed method against the state-of-the-art and baseline methods [12], [42]. In both datasets, the EEG signals were downsampled to 256 Hz, and a notch filter at 50 Hz was applied to avoid the influence of power line interference.

Both datasets have the same acquisition paradigm. Subjects sat on a chair and a screen was in front of the subjects. EEG signals were acquired from the channels on the brain scalp. The channels used in the classification include FC_z, C_3, C_z, C_4, CP_z, F_3, F_z, F_4, P_3, P_z and P_4. At the start of a trial, the screen displayed a cross. Two seconds later, a cue appeared on the screen indicating a motion of the upper limb which the subjects were then supposed to execute. In dataset I, the executed motions include *elbow flexion*, *elbow extension*, *supination*, *pronation*, *hand open*, *hand close* and the *resting* state. Dataset II includes *supination*, *pronation*, *hand open*, *palmar grasp* and *lateral grasp*. In both datasets, The number of trials for each motion were 60 and 72, and the numbers of subjects were 15 and 9, respectively.

Although both datasets have the same paradigm, the time windows of the EEG signals in the two datasets are different. In dataset I, the hand trajectory was simultaneously acquired along with the EEG signals. The movement onset of the executed motions can be located by the hand trajectory. The time window in which the EEG signals will be used for classification purposes lies between one second before the onset and one second after the onset. In dataset II, however, the hand trajectory was not recorded and there is no information about the movement. Therefore, here the time window for the classification corresponds to the two-second window after the cue indicating the start of the executed motions.

The movement onset is located with the movement trajectory in dataset I. The same localization process as in [27] was adopted and the detail about this process is given in the supplementary materials.

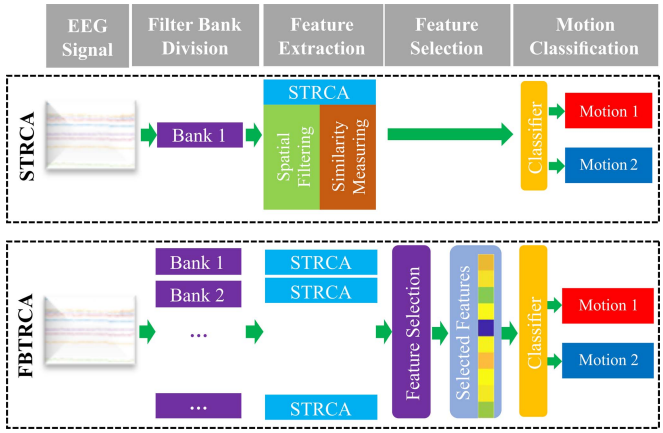

Fig. 2. Relationship between the structure of bSTRCA and bFBTRCA. The STRCA in this figure is either the bSTRCA or the mSTRCA. Both bSTRCA and mSTRCA have two steps: spatial filtering and similarity measuring. The bFBTRCA or mFBTRCA is developed by applying bSTRCA/mSTRCA to multiple banks and enabling feature selection on the features of these banks.

B. Binary FBTRCA

The proposed multi-class FBTRCA (mFBTRCA) is developed based on the binary FBTRCA (bFBTRCA). To present the relationship these two methods, we first introduce the structure of bFBTRCA and then detail how mFBTRCA is developed based on bFBTRCA.

The bFBTRCA method is developed by incorporating filter bank selection into the bSTRCA method. The key idea of bFBTRCA is to find the best frequency band in which the bSTRCA method has the best classification performance. Instead of selecting the best frequency band, bFBTRCA selects the best features from features in all frequency bands. The bFBTRCA method first divides EEG signals into multiple filter banks in the low-frequency domain. In each filter bank, bSTRCA calculates the canonical correlation pattern and uses them as the features. In bFBTRCA, the features extracted using bSTRCA in all filter banks are sorted and selected through the minimum redundancy maximum relevance method. Finally, the support vector machine classifies the selected features. The relationship between bSTRCA and bFBTRCA is shown in Fig. 2. The bFBTRCA method has three key points in the classification: (1) the spatial filtering with task-related component analysis, (2) the feature extraction from the canonical correlation pattern, and (3) filter bank selection.

1) Spatial Filtering: Because EEG signals are multi-channel signals and the channels are isolated points on the brain scalp, EEG signals naturally have a bad spatial quality. Spatial filtering is commonly used to optimize the spatial quality when processing EEG signals. A spatial filter is used to find a matrix $\boldsymbol{W} \in \mathbb{R}^{C\times P}$, where C is number of channels and $P \leq C$. By multiplying the given EEG signal $\boldsymbol{X} \in \mathbb{R}^{C\times T}$ with the matrix $\boldsymbol{W}$, the spatial-filtered signal $\boldsymbol{X}^T\boldsymbol{W} \in \mathbb{R}^{T\times P}$ is obtained. Here, T is the number of sample points. Compared to the original EEG

signal $\boldsymbol{X}$, the dimension of the spatial-filtered signals $\boldsymbol{X}^T\boldsymbol{W}$ is suppressed. The calculation methods of the spatial filter differ for different brain activities. For example, CSP is widely used in motor imagery, which aims to discern between the channels with the biggest and smallest variances [31]. In steady-state visual evoked potentials, the discriminative canonical pattern matching method is used to maximize the between-class difference and minimize the within-class difference [43]. In the bSTRCA and bFBTRCA methods, the task-related component analysis is used as the spatial filter, thereby extracting the task-related components.

Task-related component analysis optimizes the signals based on covariances of the EEG signals. The training set of EEG signals is given as $\mathcal{X}_k = \{\boldsymbol{X}_1^k, \boldsymbol{X}_2^k, \ldots, \boldsymbol{X}_{I_k}^k\}$, where k is the index of classes; for instance, in binary classification, $k = 1, 2$. I_k represents the number of trials of class k. $\boldsymbol{X}$ are multi-channel EEG signals of size $C \times T$. The task-related component analysis first computes the covariance of the intra-trial and inter-trial of each class. The intra-trial covariance is

$$\boldsymbol{C}_i^k = \boldsymbol{X}_i^k(\boldsymbol{X}_i^k)^T, \tag{1}$$

while the inter-trial covariance is given by

$$\boldsymbol{C}_{i,j}^k = \boldsymbol{X}_i^k(\boldsymbol{X}_j^k)^T + \boldsymbol{X}_j^k(\boldsymbol{X}_i^k)^T. \tag{2}$$

The spatial filter is the combination of eigenvectors, which is obtained by solving the following eigen equation:

$$\max_{\boldsymbol{\omega}} J^k = \frac{\boldsymbol{\omega}^T\boldsymbol{S}^k\boldsymbol{\omega}}{\boldsymbol{\omega}^T\boldsymbol{Q}^k\boldsymbol{\omega}}. \tag{3}$$

$\boldsymbol{S}^k$ is the sum of inter-trial covariances of class k

$$\boldsymbol{S}^k = \sum_{i,j=1,i<j}^{I_k} \boldsymbol{C}_{i,j}^k, \tag{4}$$

and $\boldsymbol{Q}^k$ is the sum of the intra-trial covariances of class k

$$\boldsymbol{Q}^k = \sum_{i=1}^{I_k} \boldsymbol{C}_i^k. \tag{5}$$

The eigen equation $\max_{\boldsymbol{\omega}} J^k$ can be solved with the generalized Schur decomposition as the generalized eigenvalue problem. The eigenvectors related to the maximal eigenvalues are denoted as $\boldsymbol{\omega}_k \in \mathbb{R}^{C\times P}$, where P is the number of fetched eigenvectors. The spatial filter of task-related component analysis, W, is the concatenation of eigenvectors of two classes $\boldsymbol{W} = [\boldsymbol{\omega}_1, \boldsymbol{\omega}_2] \in \mathbb{R}^{C\times 2P}$. The optimized calculation step of the task-related component analysis can be found in [44].

2) Similarity Measurement: In MRCP, the grand average MRCP is the mean of EEG signals across trials, denoted as:

$$\hat{\boldsymbol{X}}^k = \sum_{i=1}^{I_k} \boldsymbol{X}_i^k / I_k. \tag{6}$$

When measuring the relationship between the grand average MRCP, $\hat{\boldsymbol{X}}^k$, and each of the trials $\boldsymbol{X} \in \mathbb{R}^{C\times T}$, bSTRCA and bFBTRCA both use the canonical correlation pattern to measure the similarity. The canonical correlation pattern includes three correlation coefficients:

1) Correlation between $\boldsymbol{X}$ and $\hat{\boldsymbol{X}}^k$:

$$\boldsymbol{X}_* = \boldsymbol{X}; \boldsymbol{X}_k = \hat{\boldsymbol{X}}^k; \tag{7}$$

$$\rho_{1,k} = corr(\boldsymbol{X}_*^T\boldsymbol{W}, \boldsymbol{X}_k^T\boldsymbol{W}); \tag{8}$$

2) Correlation between $\boldsymbol{X}$ and $\hat{\boldsymbol{X}}^k$ after canonical correlation analysis:

$$\boldsymbol{X}_* = \boldsymbol{X}; \boldsymbol{X}_k = \hat{\boldsymbol{X}}^k; \tag{9}$$

$$[\boldsymbol{A}_k, \boldsymbol{B}_k] = cca(\boldsymbol{X}_*^T\boldsymbol{W}, \boldsymbol{X}_k^T\boldsymbol{W}); \tag{10}$$

$$\rho_{2,k} = corr(\boldsymbol{X}_*^T\boldsymbol{W}\boldsymbol{B}_k, \boldsymbol{X}_k^T\boldsymbol{W}\boldsymbol{B}_k); \tag{11}$$

3) Correlation between $\boldsymbol{X} - \hat{\boldsymbol{X}}^k$ and $\hat{\boldsymbol{X}}^{3-k} - \hat{\boldsymbol{X}}^k$ after canonical correlation analysis:

$$\boldsymbol{X}_* = \boldsymbol{X} - \hat{\boldsymbol{X}}^k; \boldsymbol{X}_k = \hat{\boldsymbol{X}}^{3-k} - \hat{\boldsymbol{X}}^k; \tag{12}$$

$$[\boldsymbol{A}_k, \boldsymbol{B}_k] = cca(\boldsymbol{X}_*^T\boldsymbol{W}, \boldsymbol{X}_k^T\boldsymbol{W}); \tag{13}$$

$$\rho_{3,k} = corr(\boldsymbol{X}_*^T\boldsymbol{W}\boldsymbol{A}_k, \boldsymbol{X}_k^T\boldsymbol{W}\boldsymbol{A}_k); \tag{14}$$

In the above equations, $corr$ corresponds to the two-dimensional Pearson correlation coefficient, and the function symbol cca computes the canonical coefficients for the two input data matrices. $\hat{\boldsymbol{X}}^{3-k}$ denotes the grand average MRCP of the other class ($k = 1, \hat{\boldsymbol{X}}^{3-k} = \hat{\boldsymbol{X}}^2; k = 2, \hat{\boldsymbol{X}}^{3-k} = \hat{\boldsymbol{X}}^1$). Because the canonical correlation analysis is used in the feature extraction, the EEG signals must be z-normalized before spatial filtering in bSTRCA [45], [46]. The correlations between EEG signals $\boldsymbol{X}$ and the grand average MRCPs of two classes are calculated in the binary classification. The number of correlation features is six.

3) Filter Bank Selection: In bFBTRCA, the filter bank selection consists of two steps: filter bank division and feature selection. After the z-normalization of the original EEG signals, these are divided into subbands in the low-frequency domain. The low cut-off frequencies of these subbands are fixed to 0.5 Hz, while their high cut-off frequencies are in the arithmetic sequence going from 1 Hz to 10 Hz with a 1 Hz step. Therefore, ten filter banks are used in our work.

In each filter bank, bSTRCA is used to extract features. This feature extraction includes spatial filtering and correlation coefficient extraction. The number of features is 6 in each subband, giving a total of 60 features from all subbands.

The adopted feature selection method is the minimum-redundancy maximum-relevance, which is used to select essential features from the total 60 features. Mutual information measures the mutual dependence between two variables, and it quantifies the information from one variable by observing the other variable. In the minimum-redundancy maximum-relevance, relevance is the mutual information between the label and the features, while redundancy is the mutual information between two features. The minimum-redundancy maximum-relevance method optimizes the sequence of features by minimizing the

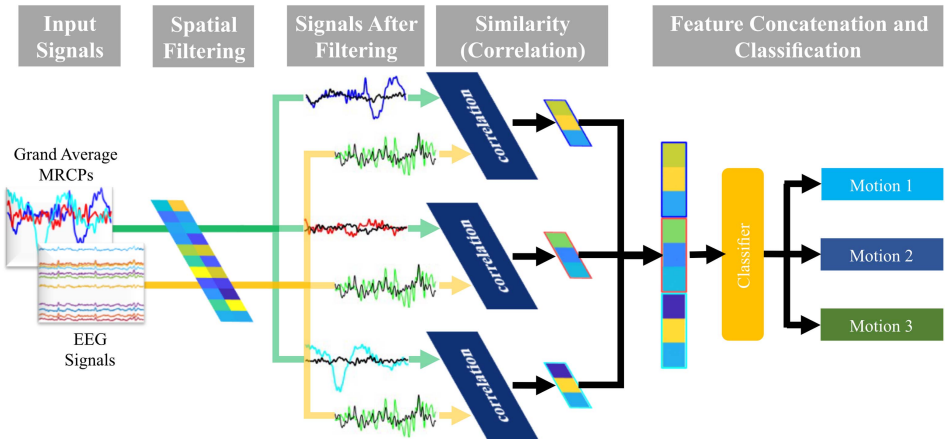

Fig. 3. Structure of the mSTRCA method for the three-class classification problem. This structure can be extended to a classification model for K classes, where $K \in \mathbb{Z}^+$. The optimization of the bSTRCA includes two main points. The first is the optimization of the spatial filter, which avoids the dimensional increase of EEG signals in multi-class classification. The second is the input of the correlation. The same components are removed from the signals after spatial filtering when measuring the similarity between the grand average MRCPs and the EEG signals, as given in (16). The proposed mFBTRCA method incorporates the filter bank selection into mSTRCA. This procedure is given in Fig. 2.

redundancy and maximizing the relevance. The selected features are then classified by the binary support vector machine classifier.

C. Multi-Class FBTRCA

The bFBTRCA method is designed to classify two states of limb movement based on the differences between grand average MRCPs of two states. When adapting the bFBTRCA to solve the multi-class classification problem, the spatial filter's structure restricts the framework's extension.

In the spatial filtering of binary classification, eigenvectors $\boldsymbol{\omega}_1 \in \mathbb{R}^{C\times P}$ and $\boldsymbol{\omega}_2 \in \mathbb{R}^{C\times P}$ of two classes are concatenated into the spatial filter $\boldsymbol{W} \in \mathbb{R}^{C\times 2P}$ used in bFBTRCA. In the K-class classification, the size of the spatial filter $\boldsymbol{W}$ is $\in \mathbb{R}^{C\times KP}$, where K is the number of classes. In this case, the number of channels KP after spatial filtering is greater than the number of channels C of the original EEG signals. After having been filtered with $\boldsymbol{W} \in \mathbb{R}^{C\times KP}$, the EEG signals are not full-rank, and therefore contain more redundant information than the original EEG signals before spatial filtering. The framework of bFBTRCA is optimized to fit with the multi-class classification.

This optimization includes two points: the spatial filter and the similarity measurement. After the optimization, the bSTRCA method can be used in the multi-class classification, which is the multi-class standard task-related component analysis (mSTRCA) method. The mFBTRCA method is developed by applying the filter bank selection to the mSTRCA method. The structure of the mSTRCA is shown in Fig. 3, using three-class classification as an example.

1) Spatial Filtering: The bSTRCA is a method developed based on the grand average MRCP. Before optimizing the frame of bSTRCA, it is necessary to clarify the relation between bSTRCA and the grand average MRCP. The grand average MRCP is the mean of EEG trials in the same class. There are three kinds of inputs involved in the calculation of the correlation coefficients in bSTRCA:

1) each of the EEG trials before averaging
2) the grand average MRCP of one class
3) the grand average MRCP of the other class.

The binary classification is based on the differences between the two grand average MRCPs. The features in bSTRCA use the similarities between each EEG trial as well as the two grand average MRCPs with correlation coefficients. The labels of the EEG trials can be predicted by their similarity. However, the noise in EEG signals are not eliminated by taking the mean of all trials. bSTRCA uses the task-related component analysis as a spatial filter to reject the task-unrelated components such as noise from the original EEG signals. Therefore, the spatial filter plays a main role in rejecting noise here, and is not related to discriminating the classes of EEG signals.

In bSTRCA, the eigenvectors of two classes are obtained by solving the eigen equation in (3) and are then concatenated into the used spatial filter. However, it is not necessary to label the eigenvectors in the spatial filter, because the filter is used for noise rejection and task-related component extraction. Since the spatial filter is responding to the noise rejection and is not related to the classification, the spatial filter used in bSTRCA is modified such that it only removes the information about classes in the spatial filter.

The summed-up inter-trial covariance $\boldsymbol{S}^k$ and the summed-up intra-trial covariance $\boldsymbol{Q}^k$ are obtained through (4) and (5). The spatial filter for the multi-class classification is found using the eigen equation

$$\max_{\boldsymbol{\omega}} J = \frac{\boldsymbol{\omega}^T \boldsymbol{S} \boldsymbol{\omega}}{\boldsymbol{\omega}^T \boldsymbol{Q} \boldsymbol{\omega}}, \tag{15}$$

where $\boldsymbol{S} = \sum_{k=1}^{K} \boldsymbol{S}^k$ and $\boldsymbol{Q} = \sum_{k=1}^{K} \boldsymbol{Q}^k$. K is the number of classes in the multi-class classification.

2) Similarity Measurement: In binary classification, the performance is determined by the differences between the grand average MRCP of two motions. When two grand average MRCPs have large differences, this indicates that the classification

accuracy of the two motions is higher than that with minor differences. To reduce the similarity between two grand average MRCPs, a possible approach is to remove the mean of the two from both grand average MRCPs. The differences between two grand average MRCPs are then maximized. In the multi-class task, the mean of grand average MRCPs of K motions are removed from the grand average MRCP $\hat{\boldsymbol{X}}^k$ and the input EEG signals $\boldsymbol{X}$ in (7), (9) and (12)

$$\boldsymbol{X} \rightarrow \boldsymbol{X} - \frac{1}{K}\sum_{k=1}^{K}\hat{\boldsymbol{X}}^k; \hat{\boldsymbol{X}}^k \rightarrow \hat{\boldsymbol{X}}^k - \frac{1}{K}\sum_{k=1}^{K}\hat{\boldsymbol{X}}^k. \quad (16)$$

The canonical correlation pattern consists of three correlation coefficients for each class in multi-class classification. The first two correlation coefficients are the same as the ones given in (8) and 11. The third one is given by (14). However, to fit with the needs of multi-class classification, (12) is replaced with

$$\boldsymbol{X}_* = \boldsymbol{X} - \hat{\boldsymbol{X}}^k; \boldsymbol{X}_k = \frac{1}{K-1}\sum_{kk=1,kk\neq k}^{K}\hat{\boldsymbol{X}}^{kk} - \hat{\boldsymbol{X}}^k. \quad (17)$$

In (12), $\boldsymbol{X}_k$ is the distance between $\hat{\boldsymbol{X}}^1$ and $\hat{\boldsymbol{X}}^2$. The distances between $\boldsymbol{X}$ and the grand average MRCPs, namely $\boldsymbol{X} - \hat{\boldsymbol{X}}^1$ and $\boldsymbol{X} - \hat{\boldsymbol{X}}^2$, are normalized by the correlation with $\hat{\boldsymbol{X}}^1$ and $\hat{\boldsymbol{X}}^2$. In the multi-class classification, $\hat{\boldsymbol{X}}^k$ is given in (17) to normalize the distance $\boldsymbol{X}_*$.

In a K-class classification, there are K grand average MRCPs $\hat{\boldsymbol{X}}^k$. For each grand average MRCP, three correlation coefficients are calculated. Therefore, there are $3K$ coefficients in each filter bank. In the binary classification, $K = 2$ and there are six features in each filter bank.

3) Filter Bank Selection: In the filter bank selection of mFBTRCA, the same setting is used as the one presented in Section II-B3. EEG signals are divided into ten filter banks, and the minimum-redundancy maximal-relevance method is used to optimize the sequence of features and select the best features for classification. The selected features are classified using the multi-class support vector machine method.

D. Comparison Methods

We compare the proposed method to both the state-of-the-art methods and the baseline methods. The state-of-the-art methods refer to the methods that have been proposed and validated in previous researches. Because the neural network is a universal solution to data processing and has no specific model, we summarize previous neural network architectures on EEG processing. The baseline methods are the networks designed under the summarized architecture. The details about these methods are given in the supplementary materials.

1) State-of-The-Art Methods: The following is a brief introduction to the compared state-of-the-art models on the multi-class classification of limb movements. All the given methods were implemented on the same datasets used in this article, including mCSP+LDA [37], SpoC+Ridge [47], MDM [48], TSLDA [48], SCNN and DCNN [49], WaveNet [50], HopeFullNet [51].

2) Baseline Methods: As EEG signals are multi-channel time series, it is unavoidable to discuss their temporal characteristics. RNN is a universal solution to the feature extraction of time series. Along with the state-of-the-art methods presented above, our model is also compared with models that combine the RNN and CNN layers. In previous EEG signal analyses, CNN was used to extract features from EEG data; the extracted features were then processed by the RNN layers to extract the temporal features, and and finally the fully connected layer was used as the classifier [52], [53]. The baseline methods follow these steps in previous analysis. Four models are compared in this work, including (1) C-R-CNN, (2) the convolutional-GRU-convolutional neural network (C-G-CNN), (3) convolutional-LSTM neural network (C-L-CNN) and (4) Graph C-G-CNN (GC-G-CNN).

3) Parameter Settings: The performance of the proposed and the compared methods are evaluated by 10-fold cross-validation. The compared methods contain various neural networks, including *SCNN* [49], *DCNN* [49], *Wavenet* [50], *HopeFullNet* [51] and the baseline methods. The compared neural networks have the same hyper-parameters, including batch size (50), learning rate (0.001) and training epochs (50). The loss function is the cross-entropy, and optimized by Adam optimizer. Both datasets are split based on the 10-fold cross-validation. The performance of all these methods is evaluated by the classification accuracy averaged from the 10 folds. All statistical analyses were conducted without correction for multiple comparisons.

III. Result

In this work, the mFBTRCA method is proposed to solve the multi-class classification problem of upper limb movements. Two datasets are used to evaluate and compare the proposed methods' performance against state-of-the-art and baseline methods. The results analysis consists of three parts: (1) the performance comparison between bFBTRCA and mFBTRCA in the binary classification task, (2) the evaluation of a three-class classification including two limb motions and the *resting* state, and (3) the multi-class classification performance evaluation. The first and second parts are evaluated and analyzed with EEG signals in dataset I. In the third part, both datasets are used to analyze the relationship between the classification accuracy and the grand average MRCP of each motion.

A. Structure Comparison

This work optimizes the spatial filter and similarity measurement of bFBTRCA such that the resulting mFBTRCA method can be used in multi-class classification. Before applying mFBTRCA to multi-class classification tasks, it is necessary to compare the performances of bFBTRCA and mFBTRCA in the binary classification task. Therefore, the bFBTRCA and mFBTRCA methods are applied to classify motion pairs in dataset I.

Fig. 4 gives the classification accuracies summarized from 10 folds of 15 subjects and 21 motion pairs. Fig. 6 shows the accuracy comparison of each motion pair. '1' refers to the case that removing the mean of grand average MRCPs (16) is not

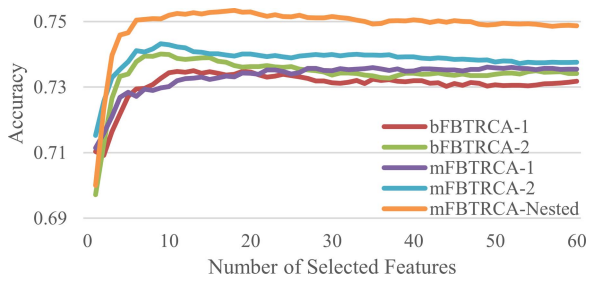

Fig. 4. Averaged accuracies across all subjects and folds. 'FBTRCA-1' denotes that the (16) is not used; 'FBTRCA-2' denotes that the (16) is not used. In 'mFBTRCA-Nested', the hyper-parameter P is determined by nested cross-validation and the (16) is used.

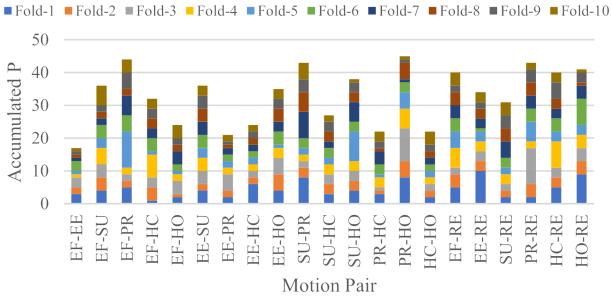

Fig. 5. Hyperparameter P values determined by nested cross-validation in the frequency range 0.5∼10 Hz for Subject 1. The values of P in this figure are calculated for 10 folds and 21 pairs of movement, respectively. The hyperparameter values of P from the 10 folds are accumulated and stacked on the graph in different colors to be adequately visualized.

used; '2' refers to the case that the (16) is used. In the spatial filter of both bFBTRCA and mFBTRCA, the number of selected eigenvectors P is 3 [27].

We also test the nested cross-validation when determining the selected eigenvectors P in mFBTRCA-Nested. Because the mFBTRCA consists of filter banks, the optimal P in each filter banks may be different. The mSTRCA is used to determine the P for each filter banks. The mFBTRCA-Nested shows a better performance than the other methods. In Fig. 5, the optimal P of Subject 1 in 0.5∼10 Hz are visualized by a stacked column chart. In the chart, the optimal P may be different between two arbitrary motions. Therefore, compared to giving a fixed value, determining P by nested cross-validation is a better approach.

In Fig. 4, the use of (16) increases the averaged accuracy about 1% when the maximum accuracy is reached, where the number of selected features is about 10. The nested cross-validation increases the averaged accuracy about 1%. To avoid further discussion on the hyper-parameters P and the number of selected features, we use the nested cross-validation to determine P and set the number of selected features to the maximum. In Table I, the averaged accuracies and p-values are given when the number of selected features is the maximum. The p-values is the results of two-sample t-test between the nested mFBTRCA and the others. The chance level is calculated with the dummy classifier with scikit-learn package in python. Both bFBTRCA and mFBTRCA methods achieve similar classification accuracies in the binary classification task.

TABLE I
ACCURACY AND p-VALUE COMPARISON IN BINARY CLASSIFICATION

	Accuracy	p-value
Chance Level	0.5197±0.0000	0.0619
bFBTRCA-1	0.7318±0.1242	0.5724
bFBTRCA-2	0.7342±0.1263	0.5898
mFBTRCA-1	0.7355±0.1233	0.5431
mFBTRCA-2	0.7376±0.1256	0.5845
mFBTRCA-Nested	0.7487±0.1250	-

B. Three-Class Comparison

This three-class comparison is carried out based on the classification accuracy between motion pairs of movement states and the $resting$ state. In Fig. 7, the classification performances of the proposed mFBTRCA method and the state-of-the-art methods are given. Table II is the p-value between mFBTRCA and the other methods, calculated with two-sample t-test. The p-values between mFBTRCA and the chance level are almost zeros, so they are not presented in this table. As can be observed, the SCNN and DCNN methods have a comparable performance to mFBTRCA. However, the process going from EEG signals to the classification features in SCNN and DCNN is ambiguous due to the interpretability of neural networks; we know that the performance of the deep neural network is good, but do not know how the network utilizes the information in the EEG signals. For the proposed mFBTRCA method, on the other hand, it is clear how the MRCP signals are transformed into features. The method removes noise via the spatial filter and measures the similarity via the correlation coefficients.

C. Multi-Class Comparison

In the results analysis of the multi-class comparison, the performance of the proposed mFBTRCA method is compared to the state-of-the-art methods and the baseline methods with EEG signals from both datasets.

a) Overall Comparison: The overall performances of the mFBTRCA method and the compared models are summarized in Table III, where the accuracies are averaged across all subjects and folds of each dataset. In this table, we apply FBTRCA to 10 bands, which have the low cut-off of 0.5 Hz and the high cut-offs of a arithmetic sequence from 1 Hz to 10 Hz with step of 1 Hz. In dataset I, mFBTRCA improves on the classification accuracy of SCNN by 6.03% ($p = 0.1258$). Furthermore, in dataset II, mFBTRCA improves on the classification accuracy of GC-G-CNN by 8.73% ($p = 0.0736$).

IV. DISCUSSION

The mFBTRCA method is developed by extending our previous bFBTRCA method, which is a binary classification model. However, there is a drawback involved when migrating from binary to multi-class classification for the bFBTRCA. The spatial filter in bFBTRCA is obtained by concatenating the eigenvectors of two classes. In the multi-class classification, the number of classes increases such that the number of eigenvectors in the spatial filters also increase. However, the number of eigenvectors

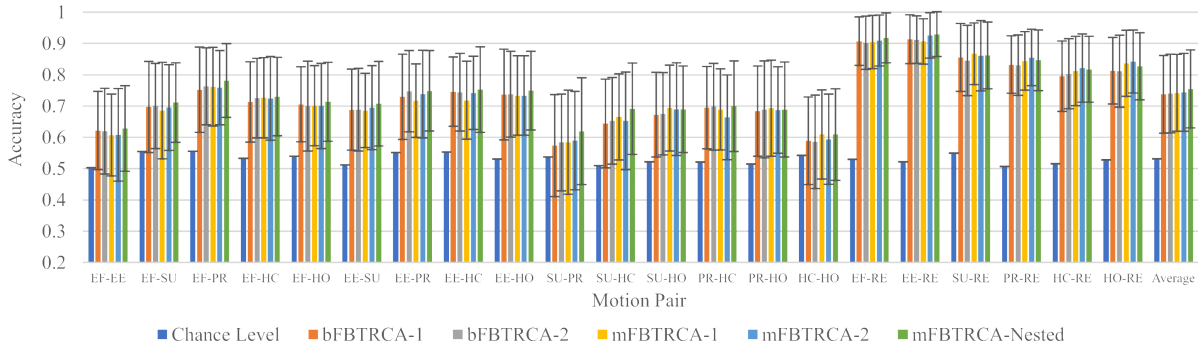

Fig. 6. Comparison of the classification accuracies between the bFBTRCA and mFBTRCA methods in the binary classification task. The abbreviations on the x-axis refer to the motion names; for instance, 'EE' is the abbreviation for *elbow extension*. The evaluation is based on the 21 motion pairs in dataset I. Accuracies are averaged across ten folds of 15 subjects. The mFBTRCA method performs similarly to bFBTRCA in binary classification.

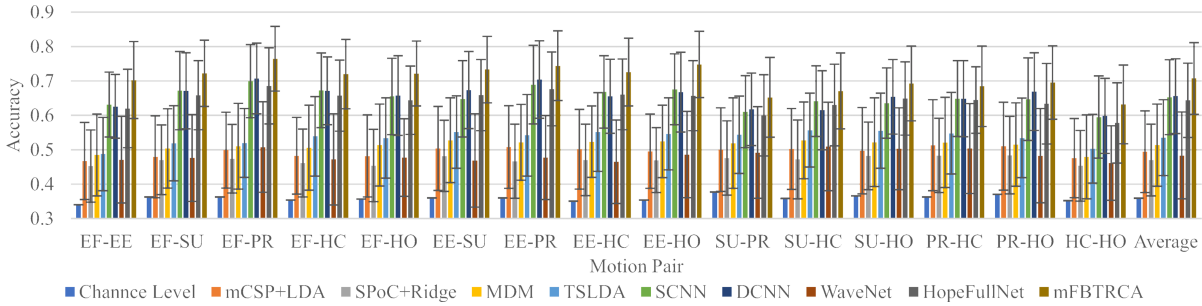

Fig. 7. Three-class classification performance comparison between the proposed mFBTRCA method and the state-of-the-art methods. The three classes in this figure are the motion pairs of limb movements and the $resting$ state. The labels on the x-axis represent the name of the motion pairs, and the name for the $resting$ state, 'RE', is ignored. The mFBTRCA method has a comparable performance to the SCNN and DCNN methods.

TABLE II
THE p-VALUE OF THREE-CLASS CLASSIFICATION

	EF-EE	EF-SU	EF-PR	EF-HC	EF-HO	EE-SU	EE-PR	EE-HC	EE-HO	SU-PR	SU-HC	SU-HO	PR-HC	PR-HO
mCSP+LDA	0.0143	0.0016	0.0006	0.0079	0.0216	0.0108	0.0030	0.0029	0.0013	0.1504	0.0639	0.0146	0.0735	0.0603
SPoC+Ridge	0.0043	0.0004	0.0031	0.0009	0.0008	0.0013	0.0008	0.0015	0.0045	0.0368	0.0268	0.0199	0.0053	0.0061
MDM	0.0251	0.0018	0.0018	0.0131	0.0069	0.0507	0.0097	0.0160	0.0029	0.0997	0.0871	0.0446	0.0862	0.0626
TSLDA	0.0132	0.0180	0.0192	0.0382	0.0547	0.0133	0.0294	0.0552	0.0663	0.1970	0.1630	0.1339	0.1203	0.0421
SCNN	0.2793	0.3313	0.3570	0.3449	0.3270	0.2106	0.3649	0.3188	0.2157	0.3584	0.3937	0.2610	0.4876	0.3795
DCNN	0.2186	0.3967	0.3110	0.4279	0.3026	0.3527	0.4888	0.2453	0.2080	0.3852	0.3401	0.3884	0.4794	0.5751
WaveNet	0.0218	0.0012	0.0127	0.0021	0.0125	0.0009	0.0015	0.0055	0.0167	0.0637	0.0941	0.0654	0.0586	0.0055
HopeFullNet	0.2924	0.2424	0.3313	0.2140	0.1394	0.2066	0.3284	0.2837	0.1709	0.4383	0.3383	0.4301	0.3918	0.3317

TABLE III
COMPARISON WITH THE STATE-OF-THE-ART AND BASELINE METHODS

Method		Performance (Mean±Std (p-value))	
		Dataset I (7 Classes)	Dataset II (5 Classes)
Chance Level	-	0.1594±0.0000 (0.0000)	0.2000±0.0000 (0.00007)
mCSP+LDA	[37]	0.2313±0.0551 (0.0037)	0.2667±0.0797 (0.0559)
SPoC+Ridge	[47]	0.2207±0.0497 (0.0006)	0.2387±0.0562 (0.0318)
MDM	[48]	0.2550±0.0700 (0.0032)	0.2768±0.0756 (0.0681)
TSLDA	[48]	0.2712±0.0631 (0.0053)	0.2892±0.0686 (0.1129)
SCNN	[49]	0.3590±0.0645 (0.1258)	0.3083±0.0640 (0.1103)
DCNN	[49]	0.3529±0.0740 (0.1287)	0.2975±0.0748 (0.0458)
WaveNet	[50]	0.2027±0.0569 (0.00005)	0.2327±0.0561 (0.0053)
HopeFullNet	[51]	0.3377±0.0774 (0.0835)	0.2292±0.0534 (0.0002)
C-R-CNN		0.3116±0.0705 (0.0374)	0.2971±0.0705 (0.0312)
C-L-CNN		0.3100±0.0654 (0.0254)	0.3121±0.0748 (0.0515)
C-G-CNN		0.3121±0.0696 (0.0184)	0.3083±0.0694 (0.0342)
GC-G-CNN		0.3177±0.0745 (0.0464)	0.3159±0.0736 (0.0726)
mFBTRCA		$\mathbf{0.4193 \pm 0.0780}$	$\mathbf{0.4032 \pm 0.0714}$

All the methods are applied on the same datasets (i and ii).
The bold values represents the best results.

in the spatial filter should be smaller than the number of channels, as otherwise the spatial filtering will increase the dimension along the channel axis of the EEG signals while keeping the rank unchanged; in other words, it would introduce useless information into the EEG signals.

The bFBTRCA method consists of three modules: spatial filtering, similarity measuring and filter bank selection. In the migration from the bFBTRCA method to the mFBTRCA method, it is assumed that spatial filtering plays the role of noise rejection, while the similarity measuring determines the classes of the EEG signals. This assumption is based on the processing of the grand average MRCP. The grand average MRCP of a class is obtained by averaging the EEG signals of that class. In MRCP signals, the class of the motions can be discriminated by comparing the differences of the grand average MRCPs. The purpose of averaging EEG signals is to remove random noise from the original signals. Therefore, the process of using the grand average MRCP

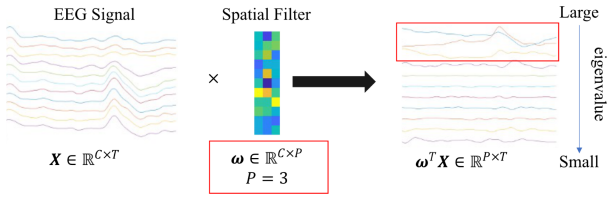

Fig. 8. EEG signals before and after spatial filtering with task-related component analysis.

to discern between different motions has two steps, (1) removing irrelevant noise from EEG signals and (2) discriminating classes by comparing the grand average MRCPs. These two steps are spatial filtering and similarity measuring, respectively.

The bFBTRCA method is migrated to mFBTRCA with this assumption. The optimization has two steps: (1) remove the steps related to the class information in the spatial filtering, and (2) reduce the similarity of the grand average MRCPs. The first step involves calculating the spatial filter with the eigenvectors given in (15), and the second step involves removing the mean of all grand average MRCPs from the spatial-filtered EEG signals in (16).

When calculating the correlation between each of the trials and the grand average MRCPs, the two inputs are spatial-filtered by task-related component analysis. Fig. 8 is an example of EEG signals before and after spatial filtering. The signals are sorted in a descending sequence of eigenvalues after spatial filtering. When the index of eigenvalues is greater than three, the signals become flat. The signals in the first three channels show distinguished fluctuation to other flat signals. This is the reason to adjust the spatial filter when immigrating the binary to the multi-class classification. In MRCP analysis, P is determined to be around 3 when the movement onset can be located. In steady-state visual evoked potential, task-related component analysis is also used in the spatial filtering of the EnsembleTRCA method [14]. The spatial filters in mFBTRCA and the EnsembleTRCA are the same. The P in steady-state visual evoked potential is set to 1 because of the high signal-to-noise ratio of steady-state visual evoked potential. However, the setting in MRCP signals is different because of the low signal-to-noise ratio. $P = 1$ cannot cover all the task-related signals. This is the reason why we don't concatenate the spatial filters of different classes as in steady-state visual evoked potential.

Although task-related component analysis may not be the most efficient tool to remove the noises, we compared it to some spatial filters in our previous work. It shows the best performance among the compared spatial filters [26]. Discriminative canonical pattern matching is the spatial filter in both steady-state visual evoked potential and MRCP [12], [43], [54]. Discriminative canonical pattern matching aims to find a projection to maximize the differences of two classes. Based on the results in [26], the performance of discriminative canonical pattern matching is much worse than task-related component analysis. Therefore, we concluded that maximizing class differences by spatially filtering should be avoided.

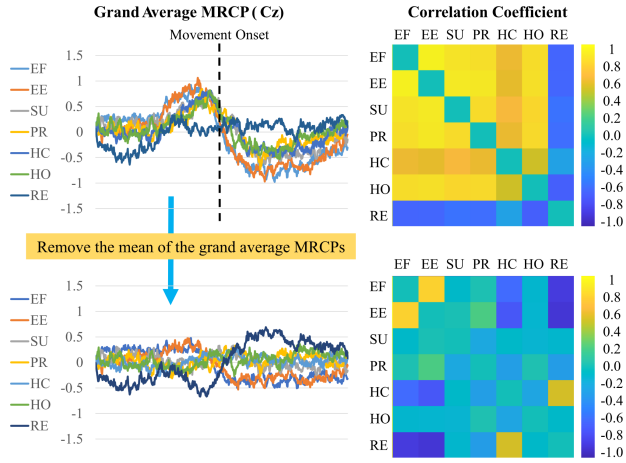

Fig. 9. Grand average MRCPs before and after removing the mean of the grand average MRCPs, and the correlation coefficients of the grand average MRCPs of the motion pairs. The time window of the EEG signals is located between one second before and after the movement onset.

In the calculation of the correlation coefficients, we remove the mean of the grand average MRCPs from both EEG trials and the grand average MRCPs in (16). In mFBTRCA, the classification performance highly relies on the differences of these grand average MRCPs. A possible approach to increase the differences is to remove the common components of these grand average MRCPs. The simplest common component is the mean of these grand average MRCPs. Fig. 9 shows the grand average MRCPs in channel C_z before and after removing the mean of the grand average MRCPs. We then calculate the correlation coefficients of the grand average MRCPs (C_z) of motion pairs. In this figure, it shows that the grand average MRCPs of the movement states are of high similarity. After removing the mean of these grand average MRCP, the correlations between motion pairs are reduced.

Now we can conclude the differences between the proposed mFBTRCA and the EnsembleTRCA. Despite of the same spatial filter in two methods, the differences between mFBTRCA and EnsembleTRCA consist of three points.

1) The filter banks. The filter bank in MRCP signals is located at the low-frequency bands. In mFBTRCA, we first divide the signals into subbands in the low-frequency bands based on our previous work [27]. In EnsembleTRCA, the filter banks are not used.
2) Added-up spatial filters instead of concatenation. As mentioned above, limited to the low signal-noise ratio of MRCP signals, mFBTRCA adds up the covariances of all the class and then solve the eigen-equation to get the spatial filter. In EnsembleTRCA, the eigen-equations are solved for the covariances of each class respectively, and then the eigenvectors of all the classes are concatenated as the spatial filter.
3) Optimized correlation features. In both mFBTRCA and EnsembleTRCA, the averaged signals across trials of each class ($\hat{\boldsymbol{X}}^k$ in 6) are used as the templates to calculate the correlation. In EnsembleTRCA, a template is

averaged of signals with a given frequency. The templates of EnsembleTRCA are of low similarity because they are located at different frequencies. However, in mFBTRCA, the templates are the same with the grand average MRCPs and are of high similarity. Therefore, mFBTRCA removes the mean of these templates before calculating the correlation.

The mFBTRCA method achieves an equivalent classification performance to the bFBTRCA method in the binary classification task, as shown in Table I. Because the binary classification between a movement state and the *resting* state (*e.g.*, *elbow flexion* vs *resting*) has a higher classification accuracy, we assume that the classification performance between the motion pairs of the movement states will not fluctuate significantly. mFBTRCA is compared to state-of-the-art methods in classifying pairs of movement states and the *resting* state (3 classes). The three-class classification accuracies are close to those achieved in the binary classification, but with slight decreases. For instance, the classification accuracy achieved between *elbow flexion*, *pronation* and *resting* is close to the one achieved between *elbow flexion* and *pronation*.

The state-of-the-art methods used in this work include machine learning-based and deep learning-based methods. The compared machine learning-based methods are geared towards the multi-class classification of limb movements, such as those made by the left/right hand, the foot or the tongue. The classification of these motions is based on certain brain activity, such as motor imagery. The deep learning technique is a universal solution to classification. Although the deep learning methods are not specific to the classification of limb movements, they have a better performance than the machine learning methods. The proposed mFBTRCA method is also based on machine learning. However, mFBTRCA takes advantage of the differences of grand average MRCPs of motions. These differences are the reason why different limb movements can be classified. As a result, mFBTRCA performs better than the deep learning methods in the multi-class classification.

Besides the state-of-the-art methods, baseline methods were designed based on deep learning to be used for comparison purposes. In the design of these, we used the same idea as when designing the mFBTRCA method, namely using spatial filtering (spatial) and similarity measuring (temporal). The CNN layers were used to optimize the spatial characteristic of EEG signals. The RNN layers were then used to extract the temporal features. Finally, the CNN layer followed by a fully connected layer was the classifier used to predict the classes of EEG signals. We compared the mFBTRCA to the state-of-the-art and baseline methods in the multi-class classification task (more than three classes). As given in Table I, mFBTRCA shows an improved performance over the other compared methods, including the baseline methods.

Although the proposed mFBTRCA method improves on the performance of the state-of-the-art and baseline methods, it also has its bottleneck. The method classifies the EEG signals based on the differences in the grand average MRCPs of motions. Importantly, when the grand average MRCPs of motions are correlated or almost the same, mFBTRCA fails to classify these motions, such as *elbow flexion* and *elbow extension*. Furthermore, the movement onset localization is a problem for armless or paralyzed patients in the actual application of the brain-computer interface. Our future work will focus on fusing the proposed mFBTRCA method with the deep learning techniques and applying transfer learning to help with the localization of the movement onset.

V. Conclusion

We propose the mFBTRCA method for the multi-class classification of upper limb movements. The proposed method is comparable to the bFBTRCA method in binary classification. In the multi-class classification task (3 classes and more), mFBTRCA has a better performance than the other compared methods, including SCNN and baseline methods based on deep learning. In the 7-class classification of dataset I, mFBTRCA improves on the performance of the best-compared method by 6.03%. In the 5-class classification of dataset II, the improvement is 8.73%. The mFBTRCA method is developed by comparing the correlation between grand average MRCPs, thus revealing the relationship between the classification performance and the grand average MRCP. This method is expected to be the baseline in future works for the multi-class classification task of upper limb movements.

References

[1] N. Mrachacz-Kersting, J. Ibáñez, and D. Farina, "Towards a mechanistic approach for the development of non-invasive brain-computer interfaces for motor rehabilitation," *J. Physiol.*, vol. 599, no. 9, pp. 2361–2374, 2021.
[2] R. A. Ramadan and A. V. Vasilakos, "Brain computer interface: Control signals review," *Neurocomputing*, vol. 223, pp. 26–44, 2017.
[3] N. Tiwari, D R. Edla, S. Dodia, and A. Bablani, "Brain computer interface: A comprehensive survey," *Biologically Inspired Cogn. Architectures*, vol. 26, pp. 118–129, 2018.
[4] M. M. Shanechi, "Brain–machine interface control algorithms," *IEEE Trans. Neural Syst. Rehabil. Eng.*, vol. 25, no. 10, pp. 1725–1734, Oct. 2017.
[5] K.-S. Hong and M. J. Khan, "Hybrid brain–computer interface techniques for improved classification accuracy and increased number of commands: A review," *Front. Neurorobot.*, vol. 11, 2017, Art. no. 35.
[6] X. Mao, W. Li, C. Lei, J. Jin, F. Duan, and S. Chen, "A brain–robot interaction system by fusing human and machine intelligence," *IEEE Trans. Neural Syst. Rehabil. Eng.*, vol. 27, no. 3, pp. 533–542, Mar. 2019.
[7] N. Guo et al., "SSVEP-Based brain computer interface controlled soft robotic glove for post-stroke hand function rehabilitation," *IEEE Trans. Neural Syst. Rehabil. Eng.*,vol. 30, pp. 1737–1744, 2022.
[8] D. Zhang, L. Yao, K. Chen, S. Wang, X. Chang, and Y. Liu, "Making sense of spatio-temporal preserving representations for EEG-Based human intention recognition," *IEEE Trans. Cybern.*, vol. 50, no. 7, pp. 3033–3044, Jul. 2020.
[9] C. Gouy-Pailler, M. Congedo, C. Brunner, C. Jutten, and G. Pfurtscheller, "Nonstationary brain source separation for multiclass motor imagery," *IEEE Trans. Biomed. Eng.*, vol. 57, no. 2, pp. 469–478, Feb. 2010.
[10] M. Tangermann et al., "Review of the BCI Competition IV," *Front. Neurosci.*, vol. 6, no. 55, pp. 1–31, 2012.
[11] H. Yang, S. Sakhavi, K. K. Ang, and C. Guan, "On the use of convolutional neural networks and augmented CSP features for multi-class motor imagery of EEG signals classification," in *Proc. IEEE 37th Annu. Int. Conf. Eng. Med. Biol. Soc.*, 2015, pp. 2620–2623.
[12] P. Ofner, A. Schwarz, J. Pereira, and G. R. Müller-Putz, "Upper limb movements can be decoded from the time-domain of low-frequency EEG," *PLos One*, vol. 12, no. 8, 2017, Art. no. e0182578.
[13] F. Duan, D. Lin, W. Li, and Z. Zhang, "Design of a multimodal EEG-based hybrid BCI system with visual servo module," *IEEE Trans. Auton. Ment. Develop.*, vol. 7, no. 4, pp. 332–341, Dec. 2015.

[14] M. Nakanishi, Y. Wang, X. Chen, Y. T. Wang, X. Gao, and T. P. Jung, "Enhancing detection of SSVEPs for a high-speed brain speller using task-related component analysis," *IEEE Trans. Biomed. Eng.*, vol. 65, no. 1, pp. 104–112, Jan. 2018.

[15] C. M. Wong, B. Wang, Z. Wang, K. F. Lao, A. Rosa, and F. Wan, "Spatial filtering in SSVEP-Based BCIs: Unified framework and new improvements," *IEEE Trans. Biomed. Eng.*, vol. 67, no. 11, pp. 3057–3072, Nov. 2020.

[16] Y. Chen, C. Yang, X. Ye, X. Chen, Y. Wang, and X. Gao, "Implementing a calibration-free SSVEP-based BCI system with 160 targets," *J. Neural Eng.*, vol. 18 no. 4, 2021 Art. no. 046094.

[17] A. Shakeel, M. S. Navid, M. N. Anwar, S. Mazhar, M. Jochumsen, and I. K. Niazi, "A review of techniques for detection of movement intention using movement-related cortical potentials," *Comput. Math. Methods Med.*, vol. 2015, pp. 1–13, 2015.

[18] I. K. Niazi, N. Jiang, O. Tiberghien, J. F. Nielsen, K. Dremstrup, and D. Farina, "Detection of movement intention from single-trial movement-related cortical potentials," *J. Neural Eng.*, vol. 8 no. 6, 2011, Art. no. 066009.

[19] I. K. Niazi, N. Jiang, M. Jochumsen, J. F. Nielsen, K. Dremstrup, and D. Farina, "Detection of movement-related cortical potentials based on subject-independent training," *Med. Biol. Eng. Comput.*, vol. 51, no. 5, pp. 507–512, 2013.

[20] J J. I. Ibáñez et al., "Detection of the onset of upper-limb movements based on the combined analysis of changes in the sensorimotor rhythms and slow cortical potentials," *J. Neural Eng.*, vol. 11 no. 5, 2014, Art. no. 056009.

[21] R. Xu, N. Jiang, C. Lin, N. Mrachacz.-Kersting, K. Dremstrup, and D. Farina, "Enhanced low-latency detection of motor intention from EEG for closed-loop brain-computer interface applications," *IEEE Trans. Biomed. Eng.*, vol. 61, no. 2, pp. 288–296, Feb. 2014.

[22] F. Karimi, J. Kofman, N. Mrachacz-Kersting, D. Farina, and N. Jiang, "Detection of movement related cortical potentials from EEG using constrained ICA for brain-computer interface applications," *Front. Neurosci.*, vol. 11, 2017, Art. no. 356.

[23] D. Liu et al., "EEG-Based lower-limb movement onset decoding: Continuous classification and asynchronous detection," *IEEE Trans. Neural Syst. Rehabil. Eng.*, vol. 26, no. 8, pp. 1626–1635, Aug. 2018.

[24] J.-H. Jeong, N.-S. Kwak, C. Guan, and S.-W. Lee, "Decoding movement-related cortical potentials based on subject-dependent and section-wise spectral filtering," *IEEE Trans. Neural Syst. Rehabil. Eng.*, vol. 28, no. 3, pp. 687–698, Mar. 2020.

[25] N. Mammone, C. Ieracitano, and F. C. Morabito, "A deep CNN approach to decode motor preparation of upper limbs from time–frequency maps of EEG signals at source level," *Neural Netw.*, vol. 124, pp. 357–372, 2020.

[26] F. Duan, H. Jia, Z. Sun, K. Zhang, Y. Dai, and Y. Zhang, "Decoding pre-movement patterns with task-related component analysis," *Cogn. Comput.*, vol. 13, pp. 1389–1405, 2021.

[27] H. Jia, Z. Sun, F. Duan, Y. Zhang, C. F. Caiafa, and J. Solé-Casals, "Improving pre-movement pattern detection with filter bank selection," *J. Neural Eng.*, vol. 19, 2022, Art. no. 066012.

[28] M. Jochumsen, I. K. Niazi, N. N. Mrachacz-Kersting, D. Jiang Farina, and K. Dremstrup, "Comparison of spatial filters and features for the detection and classification of movement-related cortical potentials in healthy individuals and stroke patients," *J. Neural Eng.*, vol. 12 no. 5, 2015 Art. no. 056003.

[29] Y. Chu et al., "Decoding multiclass motor imagery EEG from the same upper limb by combining riemannian geometry features and partial least squares regression," *J. Neural Eng.*, vol. 17 no. 4, 2020, Art. no. 046029.

[30] J. Liu, F. Ye, and H. Xiong, "Multi-class motor imagery EEG classification method with high accuracy and low individual differences based on hybrid neural network," *J. Neural Eng.*, vol. 18, no. 4, Aug. 2021, Art. no. 0460f1.

[31] Y. Zhang, C. S. Nam, G. Zhou, J. Jin, X. Wang, and A. Cichocki, "Temporally constrained sparse group spatial patterns for motor imagery BCI," *IEEE Trans. Cybern.*, vol. 49, no. 9, pp. 3322–3332, Sep. 2019.

[32] B. Liu, X. Chen, N. Shi, Y. Wang, S. Gao, and X. Gao, "Improving the performance of individually calibrated SSVEP-BCI by task- discriminant component analysis," *IEEE Trans. Neural Syst. Rehabil. Eng.*, vol. 29, pp. 1998–2007, 2021.

[33] J. Ibáñez, J. I. Serrano, M. D. del Castillo, J. Minguez, and J. L. Pons, "Predictive classification of self-paced upper-limb analytical movements with EEG," *Med. Biol. Eng. Comput.*, vol. 53, no. 11, pp. 1201–1210, 2015.

[34] M. Jochumsen, I. K. Niazi, K. Dremstrup, and E. N. Kamavuako, "Detecting and classifying three different hand movement types through electroencephalography recordings for neurorehabilitation," *Med. Biol. Eng. Comput.*, vol. 54, no. 10, pp. 1491–1501, 2016.

[35] N. Robinson and A. P. Vinod, "Noninvasive brain-computer interface: Decoding arm movement kinematics and motor control," *IEEE Syst., Man, Cybern. Mag.*, vol. 2, no. 4, pp. 4–16, Oct. 2016.

[36] B. J. Edelman, B. Baxter, and B. He, "EEG source imaging enhances the decoding of complex right-hand motor imagery tasks," *IEEE Trans. Biomed. Eng.*, vol. 63, no. 1, pp. 4–14, Jan. 2016.

[37] M. Grosse-Wentrup and M. Buss, "Multiclass common spatial patterns and information theoretic feature extraction," *IEEE Trans. Biomed. Eng.*, vol. 55 no. 8, pp. 1991–2000, Aug. 2008.

[38] W. Yi, S. Qiu, H. Qi, L. Zhang, B. Wan, and D. Ming, "EEG feature comparison and classification of simple and compound limb motor imagery," *J. NeuroEng. Rehabil.*, vol. 10, no. 1, 2013, Art. no. 106.

[39] B. Xu et al., "Wavelet transform time-frequency image and convolutional network-based motor imagery EEG classification," *IEEE Access*, vol. 7, pp. 6084–6093, 2019.

[40] M.-A. Li, Y.-F. Wang, S.-M. Jia, Y.-J. Sun, and J.-F. Yang, "Decoding of motor imagery EEG based on brain source estimation," *Neurocomputing*, vol. 339, pp. 182–193, 2019.

[41] S.-B. Lee, H.-J. Kim, H. Kim, J.-H. Jeong, S.- W. Lee, and D.-J. Kim, "Comparative analysis of features extracted from EEG spatial, spectral and temporal domains for binary and multiclass motor imagery classification," *Inf. Sci.*, vol. 502, pp. 190–200, 2019.

[42] P. Ofner, A. Schwarz, J. Pereira, D. Wyss, R. Wildburger, and G. R. Müller-Putz, "Attempted Arm and Hand Movements can be Decoded from Low-Frequency EEG from Persons with Spinal Cord Injury.," *Sci. Rep.*, vol. 9, no. 1, 2019, Art. no. 7134.

[43] M. Xu, X. Xiao, Y. Wang, H. Qi, T. P.- Jung, and D. Ming, "A brain–computer interface based on miniature-event-related potentials induced by very small lateral visual stimuli," *IEEE Trans. Biomed. Eng.*, vol. 65, no. 5, pp. 1166–1175, May 2018.

[44] H. Tanaka, "Group task-related component analysis (gTRCA): A multivariate method for inter-trial reproducibility and inter-subject similarity maximization for EEG data analysis," *Sci. Rep.*, vol. 10, no. 1, 2020, Art. no. 84.

[45] C. Cheadle, M. P. Vawter, W. J. Freed, and K. G. Becker, "Analysis of microarray data using Z score transformation," *J. Mol. Diagnostics*, vol. 5, no. 2, pp. 73–81, 2003.

[46] F. Karim, S. Majumdar, and H. Darabi, "Insights into LSTM fully convolutional networks for time series classification," *IEEE Access*, vol. 7, pp. 67718–67725, 2019.

[47] S. Dähne et al., "SPoC: A novel framework for relating the amplitude of neuronal oscillations to behaviorally relevant parameters," *NeuroImage*, vol. 86, pp. 111–122, 2014.

[48] A. Barachant, S. Bonnet, M. Congedo, and C. Jutten, "Multiclass brain–computer interface classification by Riemannian geometry," *IEEE Trans. Biomed. Eng.*, vol. 59, no. 4, pp. 920–928, Apr. 2012.

[49] R. T. Schirrmeister et al., "Deep learning with convolutional neural networks for EEG decoding and visualization: Convolutional neural networks in EEG analysis," *Hum. Brain Mapping*, vol. 38, no. 11, pp. 5391–5420, 2017.

[50] P. Thuwajit et al., "EEGWaveNet: Multiscale CNN-Based spatiotemporal feature extraction for EEG seizure detection," *IEEE Trans. Ind. Inform.*, vol. 18, no. 8, pp. 5547–5557, Aug. 2022.

[51] F C. Mattioli Porcaro and G. Baldassarre, "A 1D CNN for high accuracy classification and transfer learning in motor imagery EEG-based brain-computer interface," *J. Neural Eng.*, vol. 18 no. 6, 2021 Art. no. 066053.

[52] G. Xu, T. Ren, Y. Chen, and W. Che, "A. one-dimensional CNN-LSTM model for epileptic seizure recognition using EEG signal analysis," *Front. Neurosci.*, vol. 14, 2020, Art. no. 578126.

[53] A. Iyer, S. S. Das, R. Teotia, S. Maheshwari, and R. R. Sharma, "CNN and LSTM based ensemble learning for human emotion recognition using EEG recordings," *Multimedia Tools Appl.*, vol. 82, pp. 4883–4896, 2022.

[54] K. Wang, M. Xu, Y. Wang, S. Zhang, L. Chen, and D. Ming, "Enhance decoding of pre-movement EEG patterns for brain–computer interfaces," *J. Neural Eng.*, vol. 17 no. 1, 2020 Art. no. 016033.